International Journal of GEOMATE, Aug., 2025 Vol.29, Issue 132, pp.1-11
ISSN: 2186-2982 (P), 2186-2990 (O), Japan, DOI: https://doi.org/10.21660/2025.132.4947
Geotechnique, Construction Materials and Environment

EXPERIMENTAL STUDY ON DRYING, AUTOGENOUS AND RESTRAINED SHRINKAGE STRAINS OF ALKALI-ACTIVATED FLY ASH GEOPOLYMER CONCRETE

Viet-Tam Tran[1], * Tuan-Trung Nguyen[1], Khanh-Hung Nguyen[2] and Thanh-Tung Pham[1]

[1]Faculty of Civil and Industrial Construction, Hanoi University of Civil Engineering, Vietnam; [2]Faculty of Civil Engineering, Lac Hong University, Dong Nai, Vietnam

*Corresponding Author, Received: 16 March 2025, Revised: 02 May 2025, Accepted: 17 May 2025

ABSTRACT: This paper presents novel experimental results on the drying, autogenous, and restrained shrinkage strains of one-part alkali-activated geopolymer concrete (AAGC). Five geopolymer concrete mixtures and three ordinary Portland cement concrete mixtures were cast and studied. The impact of the ratio between the alkali activator and the total amount of fly ash and ground granulated blast furnace slag (ACT/FG), along with the total content of FG on the compressive strength and drying shrinkage of AAGC, was examined. The results indicated that the compressive strength of AAGC improved with rising calcium and silica content in the binder. The 28-day compressive strength of AAGC ranged from 31.6 MPa to 48.6 MPa. An increase in the alkaline activator from 6% to 10% can result in a 40.4% increase in compressive strength. Conversely, the amount of alkali activator had a minor impact on the drying shrinkage of AAGC. The 120-day drying shrinkage of AAGC specimens was 2.3 to 4.0 times greater than that of OPCC samples. A reinforcement ratio of 1.13% can reduce the drying shrinkage strain of AAGC by approximately 4.0 to 5.0 times. The experiment demonstrated that OPC mixtures outperformed GPC regarding the first crack appearance. The GPC mixtures cracked earlier but displayed small cracks that did not propagate towards the steel ring. The inclusion of drying, autogenous, and restrained shrinkage provides a well-rounded perspective, which is critical for structural applications of GPC.

Keywords: Geopolymer concrete; Alkali activator; Fly ash; Shrinkage strain; Sustainable

1. INTRODUCTION

Alkali-activated materials (AAMs), also known as geopolymers [1], are recognised as eco-friendly and sustainable alternatives to ordinary Portland cement (OPC) binders due to their superior engineering properties compared to OPC and their potential to reduce carbon content [2]. AAMs result from a reaction between amorphous aluminosilicates, such as ground granulated blast furnace slag (GBFS) or fly ash (FA), and an alkaline solution (activator) [3]. The properties of these materials vary depending on the type and quantity of raw materials, mixing procedure, and curing conditions.

There are two types of activators: one-part or “just add water” AAMs, and the conventional two-part AAMs [4]. The conventional AAMs, referred to as "two-part" AAMs, are created by mixing an alkaline solution with an aluminosilicate precursor [5]. This type of AAM can present challenges in transportation, storage, and mixing with raw materials. Consequently, one-part AAMs have gained widespread use, leading to numerous studies in recent times. In one-part AAMs, a powdered alkali activator is combined with amorphous aluminosilicate, requiring water to initiate the chemical reactions. The production process is akin to that of OPC, eliminating the issues associated with the alkaline solution. As a result, this innovation makes it easier to use and more popular [6, 7].

One-part alkali-activated geopolymer concrete (referred to as “AAGC” in this paper) is a type of concrete that utilises alkali-activated materials (AAMs) as a binder. This variety of concrete offers several advantages over ordinary Portland cement concrete (OPCC), including the potential for high compressive strength that can exceed 100 MPa [8] and excellent performance against fire and chemical attacks.

Despite its favourable performance compared to OPCC, applying AAGC in the industry remains questionable due to its volumetric instability, which is linked to significant autogenous and drying shrinkage strains. Autogenous shrinkage denotes the macroscopic volume reduction of binders under sealed conditions following the initial setting, while drying shrinkage refers to the volume change resulting from the evaporation of internal water from the matrix due to the humidity difference between the internal and external parts [9]. Extensive research has indicated that the final drying shrinkage of AAGC can be 1.5 to 3.5 times greater than that of OPCC specimens [10, 11]. Drying shrinkage is influenced by many internal and external factors, including binder composition, porosity, pore size distribution, type and concentration of activators, type of aggregates, and external conditions [12]. Most of these internal factors impacting the drying shrinkage of two-part alkali-activated slag concrete have been thoroughly investigated.

However, there were only a few studies on the autogenous and drying shrinkage strains of AAGC. Sageghian *et al*. [11] conducted an experimental study involving 24 design mixes to evaluate the drying shrinkage of one-part alkali-activated slag concrete up to 180 days, cured in two different environments (in water and sealed in plastic bags). They reported that nearly 75% of the 180-day shrinkage was reached within 20 days, and adding silica fume considerably reduced the drying shrinkage magnitude. Islam *et al*. [13] quantified the restrained shrinkage of geopolymer concrete using ring specimens. They discovered that along with the activator solution to fly ash ratio, the final compressive strength of GPC plays an important role in shrinkage strain.

While significant research has been conducted on the shrinkage of alkali-activated materials [11-13], a notable gap exists in the comprehensive understanding of autogenous and drying shrinkage specifically in one-part alkali-activated geopolymer concrete systems utilising fly ash and slag blend. Many existing studies have primarily focused on two-part systems or have not thoroughly investigated the influence of mix design parameters on the early-age shrinkage characteristics of the one-part concrete. Furthermore, limited research has explored the restrained shrinkage and cracking behaviour in such systems, particularly with reinforcement.

This study investigates autogenous, drying, and restrained shrinkage strains in alkali-activated geopolymer concrete (AAGC), focusing on the effects of mix design parameters such as fly ash–slag blend (“FG”) content and the alkaline activator-to-FG ratio (ACT/FG). To enable performance comparison, three ordinary Portland cement concrete (OPCC) mixes were also prepared alongside the AAGC samples, addressing key gaps in understanding shrinkage behavior across different binder systems.

2. RESEARCH SIGNIFICANCE

This research holds significant implications for advancing sustainable construction practices in Vietnam and globally. By thoroughly investigating the shrinkage behaviour of one-part alkali-activated geopolymer concrete, this study addresses a crucial aspect for structural applications of GPC. The findings on the influence of binder composition and alkaline activator content on drying, autogenous, and restrained shrinkage provide essential data for optimising mix designs and mitigating cracking risks. The demonstrated effectiveness of reinforcement in reducing shrinkage strains offers practical strategies for enhancing the durability and serviceability of geopolymer concrete structures. This work contributes to a deeper understanding of this promising alternative to conventional Portland cement, paving the way for more environmentally friendly and resilient structure development.

3. EXPERIMENTAL PROGRAMME

3.1 Materials

The fly ash (FA) used in this study is F-class, collected, dried, and packed from the Vietnam Pha Lai thermal power plant. Granulated blast furnace slag (GBFS) was finely ground, dried, and packed from the Hoa Phat steel factory in Vietnam. Both materials were tested for their chemical composition and particle size before use. The analysis results of the fly ash and blast furnace slag samples indicated that these materials met the requirements of EN 15167-1 [14]. Table 1 presents the physical properties and chemical composition.

Fly ash consists of finely divided ashes produced by pulverized coal in power plants. The chemical composition of FA includes about 30 different chemical elements, in the form of oxides such as SiO_2, Al_2O_3, CaO, MgO, Fe2O3, etc. Within them, the four oxides of SiO_2, Al_2O_3, CaO, MgO are the most important element since it decide the FA properties. The percentage of these oxides in FA depend on the mineral composition of coal. For GBFS, the main chemical compositions include CaO, MgO, SiO_2 and Al_2O_3 with the total percentage of 90% to 95%. The percentage of other oxides varies in a small range depending on chemical composition of iron ore and slag.

Table 1. Properties of FA and GBFS

Property	FA	GBFS
Physical		
Density (g/cm^3)	2.24	2.91
Surface area (cm^2/g)	3400 (Blaine)	5220 (Blaine)
Chemical composition		
SiO_2 (%)	58.70	35.02
Al_2O_3 (%)	22.87	13.56
Fe_2O_3 (%)	7.31	1.41
CaO (%)	0.98	38.6
MgO (%)	0.85	8.18
Na_2O (%)	0.33	0.31
K_2O (%)	3.6	0.80
TiO_2 (%)	1.35	0.23
MKN (%)	3.53	1.89

Alkali-Activated Materials (AAM) can be sodium hydroxide (NaOH), potassium hydroxide (KOH), sodium silicate (Na_2SiO_3) and potassium silicate (K_2SiO_3). AAM can be classified as one-part or “just add water” AAM and the conventional two-part AAM [4]. In this study, the alkali-activator is one-part AAM and supported by APTES Pty – Australia. This activator, namely M-activator, in a solid state as a white powder is a form of sodium silicate holding *n* water molecules ($Na_2SiO_3.nH_2O$). The solid activator is dryly mixed with FA and BFS before they are dissolved in water to create the binder. Using the activator in its dry state offers several advantages, including ease of maintenance and transport, and uniform contact between FA-BFS and the activator to enhance the quality of GPC. This activator has a density of 2.41 g/cm³ and a mass ratio of SiO_2/Na_2O of 2.1.

Crushed stone with a 5-10 mm grain size and river sand were used as the coarse and fine aggregates. The physical properties of the stone and sand are presented in Table 2.

Table 2. Properties of stone and sand

Property	Stone	Sand
Density in dry condition (g/cm^3)	2.73	2.63
Density at surface dry saturation (g/cm^3)	2.76	2.65
Volumetric mass in the compacted state (kg/m^3)	1586	1700
Porosity in compacted state (%)	42.9	35.0
Surface dry saturated water absorbency (%)	0.84	0.75

3.2 Concrete Mixtures and Curing

A total of five mixtures for AAGC and three mixtures for OPCC were produced. The proposed mix design of the samples is shown in Table 3, based on the extensive preliminary tests conducted by the authors [15, 16]. Two variables were examined in the AAGC mixtures. The first variable was the total amount of FA and GBFS (FG), varying from 400 to 500 kg, which aimed to study the effect of the total amount on shrinkage strain. The second variable was the ratio of activator to FG (ACT/FG), changing from 6% to 10%. The ratio of water to FG remained constant at 0.45. The AAGC mixtures were denoted by their variables. For instance, G400-6 represents an AAGC mixture with an FG amount of 400 kg and 6% of ACT to FG.

Numerous studies have investigated the effect of the FA/GBFS ratio on the compressive strength and workability of AAGC [17, 18]. The test results indicated that replacing part of GBFS with FA can enhance the compressive strength at an early age under ambient curing conditions. Therefore, this study set the FA/GBFS ratio at one-third based on the authors' previous research. For OPCC, three mixtures were produced, as outlined in Table 3. The cement content varied at 405, 461, and 515 kg per cubic metre to examine the impact of cement quantity on autogenous and drying shrinkage strains.

To produce an AAGC mixture, the powdered materials, including FA, GBFS, and activator, were mixed dry for 2 minutes. Fine aggregate was then added to the mixture and mixed for an additional 2 minutes, followed by the addition of two-thirds of the water. While the mixture was being blended, the remaining water and the coarse aggregate were gradually incorporated and mixed for 2 to 3 minutes. Finally, the samples were cast in two layers using a vibrating table. After casting, the moulds were covered with two plastic layers to prevent surface evaporation and to retain moisture until demoulding. All the specimens were demoulded one day after casting, and the measurement process commenced.

3.3 Test Specimens

3.3.1 Shrinkage test specimens

As shown in Table 4, 15 samples were cast for each design mixture to measure drying shrinkage (TS series), autogenous shrinkage (AS series), restrained shrinkage with rebar (TS-R series), compressive strength, and elastic modulus.

Table 3. Mix design of AAGC and OPCC (per m^3)

Mix design	*FA*	*GBFS*	*FG*	*C*	*Sand*	*Stone*	*ACT*	*W*	*Ratio*		
	(kg)	*(kg)*	*(kg)*	*(kg)*	*(kg)*	*(kg)*	*(kg)*	*(l)*	*ACT/FG*	*W/FG*	*W/C*
G400-6	100	300	400	-	640	1220	24	180	0.06	0.45	-
G400-8	100	300	400	-	640	1220	32	180	0.08	0.45	-
G400-10	100	300	400	-	640	1220	40	180	0.10	0.45	-
G450-8	112.5	337.5	450	-	640	1220	36	202.5	0.08	0.45	-
G500-8	125	375	500	-	640	1220	40	225	0.08	0.45	-
O-405	-	-	-	405	640	1220	-	182.25			0.45
O-461	-	-	-	461	640	1220	-	201.6			0.45
O-515	-	-	-	515	640	1220	-	231.25			0.45

Table 4. Test sample for one mixture

No.	*Test*	*Denote*	*Sample size (mm)*	*Number of samples*	*Days*
1	Drying shrinkage	TS-	100x100x400	3	2 - 120
2	Autogenous shrinkage	AS-	100x100x400	3	2 - 120
3	Restrained shrinkage with rebar (1T12)	TS-R-	100x100x400	3	2 - 120
4	Compressive strength test	C-	Cylinder 150x300	3	28
5	Elastic modulus test	Eb-	Cylinder 150x300	3	28
6	Ring test			1	2

The test samples are shown from Fig. 1 to 3. All shrinkage tests were carried out using prismatic specimens measuring 400 mm in length and 100 x 100 mm in cross-section according to Vietnamese standard TCVN 3117:2022 [19]. All specimens were demoulded one day after casting. Following demoulding, two measurement pins were attached to the samples with a gauge length of 300 mm. The autogenous shrinkage samples were tightly wrapped in plastic to prevent moisture loss. The first reading of shrinkage was taken on the second day after casting. Subsequently, the specimens were placed in an environmental control chamber.

Typically, for both drying and autogenous shrinkage, an increase in temperature generally leads to an increase in the shrinkage rate and often the final magnitude of shrinkage strain. However, the relationship is not always linear and can be influenced by other factors. On the other hand, an increase in the relative humidity of the surrounding environment leads to a decrease in drying shrinkage strain because it reduces the rate and magnitude of moisture loss from the concrete. However, the temperature and relative humidity were kept constant in this experiment to be able to compare the results. Therefore, the environmental chamber was set up at a constant temperature of 27±2°C and a relative humidity of 80±5%. This environmental condition reflects the typical weather patterns in Vietnam. Changes in specimen length were monitored at specific intervals with a digital micrometre, and the shrinkage strain was measured for up to 120 days.

The selection of prismatic specimens (100x100x400 mm) and a 300 mm gauge length adhered to the Vietnamese standard TCVN 3117:2022, ensuring the findings' applicability to local construction practices and material specifications.

Reliability was addressed through meticulous control of mixing proportions, consistent curing conditions for each mix design, and repeated measurements on multiple specimens to ensure the repeatability and precision of the shrinkage data. Validity was enhanced by isolating autogenous shrinkage through sealed specimens, effectively eliminating moisture exchange, and employing a standardised measurement procedure.

To study shrinkage strain in a restrained condition, the TS-R- samples were produced using prismatic specimens measuring 100x100x400 mm, with a single rebar of 12 mm diameter positioned at the centre of the specimen. The specimen has no restraints at both ends and is put freely and measured like other specimens.

After taking the sample from the climate chamber, a comparator measuring device was used to measure shrinkage strain (Fig. 4). Initially set to a zero value, the standard bar was placed horizontally with the concrete sample. The results were measured and calculated from the first reading after 1, 3, 7, and 14 days, and subsequently every 2 weeks until the end of the experiment. The measuring instruments were initially checked carefully, and the errors were considered negligible.

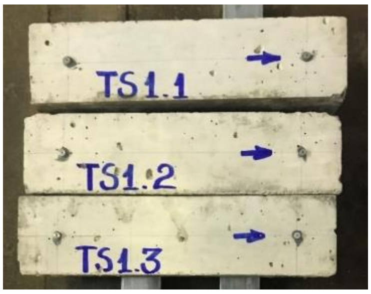

Fig. 1 Drying shrinkage samples

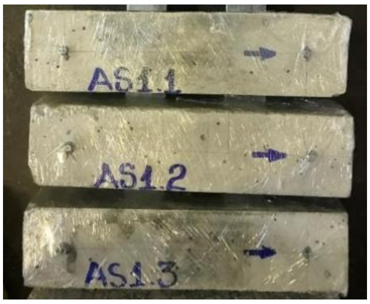

Fig. 2 Autogenous shrinkage samples

Fig. 3 Restrained shrinkage

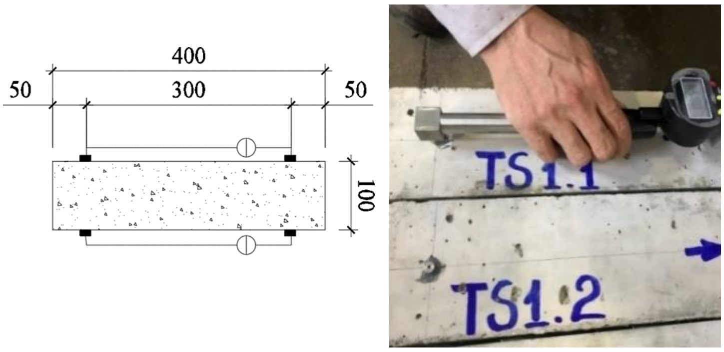

Fig. 4 Strain measurement

Fig. 5 Ring test

Shrinkage strain of each sample at the measured time can be calculated by Eq. (1):

$$\varepsilon_t = \frac{\Delta_L(t)}{L} \quad (1)$$

where $\Delta_L(t)$ is the difference in length between the measuring pins of the sample at time t compared to the original L in mm, determined by Eq. (2):

$$\Delta_L(t) = \frac{c_t - c_0}{K} \quad (2)$$

where c_0 is the reading at the initial time $t = 0$, c_t is the reading at time t (day), $K = 1000$ is the instrument amplification factor; L=300mm is the distance between the measuring pins.

For each design mix, three 150x300 cylinders were cast to perform the compressive strength test, and three additional cylinders were cast to assess the elastic modulus.

3.3.2 Ring test

The restrained shrinkage test apparatus, known as the “ring test”, was prepared following ASTM C1581 [20], as depicted in Figs. 5-6, where concrete shrinkage strain is indirectly measured via the strain of the inner steel ring. The shrinkage mechanism in this experiment can be summarised as follows: shrinkage of concrete generates a uniform pressure on the steel ring, leading to strain in the ring. Conversely, the steel ring exerts a uniform reaction force on the interior of the concrete ring, resulting in the appearance of tensile and compressive stresses in the concrete. As concrete shrinkage progresses, the pressure on the steel ring increases gradually. Thus, the reaction force on the concrete ring and the tensile stress within the concrete also rise correspondingly. When the tensile strain in the concrete reaches its limit, it will crack and lose structural integrity. The steel ring will no longer be under pressure and revert to its original state. Through this mechanism, sensors are placed to measure deformation in the steel ring, and one can observe the concrete shrinkage process.

Two AAGC and two OPCC mixtures were prepared to investigate the restrained shrinkage behaviour. The specimens were maintained in the environmental control chamber, similar to the drying shrinkage samples. The first strain measurement was conducted after 24 hours, when the outer circle was removed. Measurements were taken at 30-minute intervals until cracks appeared in the concrete ring, resulting in a sudden decrease in strain on the steel ring.

4. RESULTS AND DISCUSSIONS

The experimental programme aims to study the effects of the total amount of FG and the ACT/FG ratio on the shrinkage strain of AAGC mixtures and investigate the impact of cement content on the autogenous and drying shrinkage strains of OPCC. Autogenous, drying, and restrained shrinkage strains with rebar were measured for each design mixture. The results shown in the figures are the average values of 3 samples for each design mix.

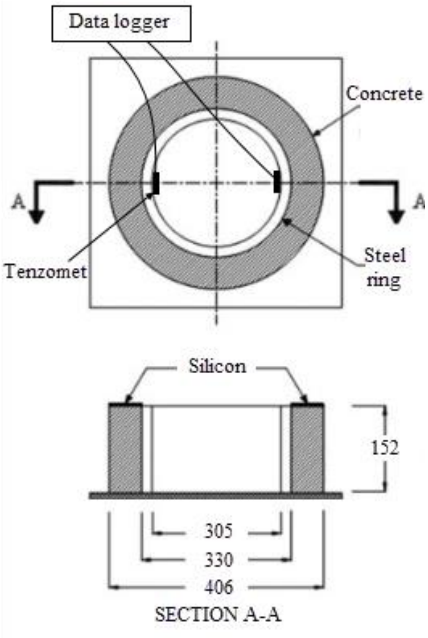

Fig. 6 Ring test schematic according to ASTM C1581

4.1 Compressive Strength

Fig. 7 shows the compressive strength development over time with 5 GPC mixes. The GPC400-6, GPC400-8, and GPC400-10 mixes correspond to ACT/FG ratios of 6%, 8%, and 10%, respectively. The compressive strength of GPC400-6 (comprising 6% fly ash and blast furnace slag) reached 31.5 MPa at 28 days, while GPC400-8 achieved 38.6 MPa (an increase of 22.5%), and GPC400-10 attained 47.1 MPa (an approximate increase of 40.4%). As the percentage of ACT/FG increases, compressive strength improves.

Fig. 7 also illustrates the compressive strength development, with the ACT/FG content maintained at a constant 8%. The compressive strength at 28 days for GPC450-8 and GPC500-8 increased by approximately 10.4% and 25.9%, respectively, compared to GPC400-8, reaching 38.6 MPa. This improvement is attributed to the higher content of FA and GBFS, which comprises about 12.5% for GPC450-8 and 25% for GPC500-8, compared to GPC400-8, resulting in increased calcium and silica content within the mixture.

Fig. 7 also shows the compressive strength development of 3 OPC mixes. The OPC-405, OPC-461, and OPC-515 mixes correspond to the cement content of 405, 461, and 515 kg, respectively. The compressive strength of OPC-405 reached 29.8 MPa at 28 days, while OPC-461 achieved 37.1 MPa (an increase of 24.5%), and OPC-515 attained 46.9 MPa (an approximate increase of 57.4%). This is reasonable since the cement content increased 13.8% and 27.16%, respectively.

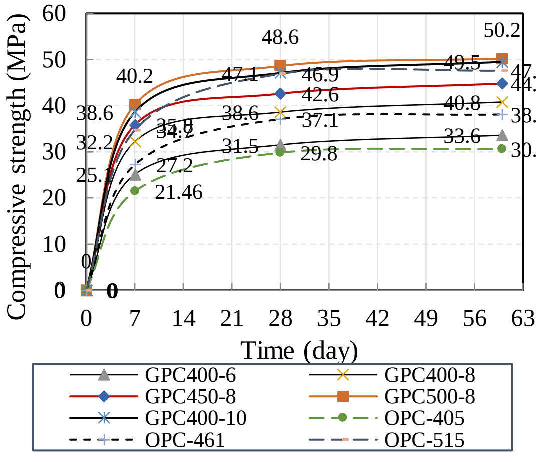

Fig. 7 Development of compressive strength

4.2 Drying And Autogenous Shrinkage Strains

The mean drying shrinkage strains of five AAGC design mixes and three OPCC design mixes are shown in Fig. 8. The results indicate that the drying shrinkage of AAGC samples was approximately 2.3 to 4.0 times higher than that of OPCC samples, similar to the previous research [21]. The 120-day drying shrinkage of AAGC specimens ranged from 815με to 1058με, whereas for OPCC specimens, the values varied between 267με and 468με. This may be attributed to a significant amount of uncombined water in alkali aluminosilicate hydrates and an increased capillary stress in AAGC structures [21].

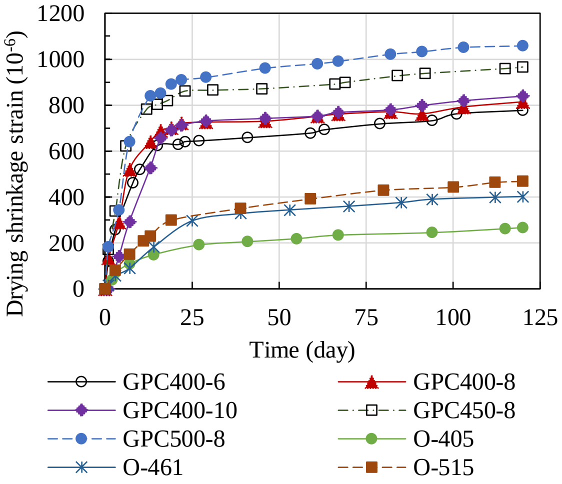

Fig. 8 Drying shrinkage strain

It is also noted that the rate of drying shrinkage was high in the first 20 to 22 days following demoulding, and thereafter, the rate slowed considerably. For AAGC samples, approximately 80% to 85% of the total 120-day drying shrinkage occurred within 22 days, whereas for OPCC, around 60% to 65% of the 120-day drying shrinkage was achieved. This aligns well with previous studies [11, 22]. The rate of drying shrinkage depends on the amount of water lost from the concrete. As water loss increases, the drying shrinkage strain rises due to greater porosity in the concrete.

Autogenous shrinkage strain is defined as the external volume contraction of concrete cured at a constant temperature and protected against water loss [22]. In this study, the autogenous shrinkage of AAGC and OPCC samples was measured using sealed specimens with dimensions of 100 x 100 x 400 mm at a constant temperature of 27 ± 2 °C and a relative humidity of 80 ± 5%. The results of the autogenous shrinkage strain are presented in Fig. 9.

The trend of autogenous shrinkage strain mirrored that of drying strain. The rate was high during the first 20 to 22 days and then progressed slowly until 120 days. The maximum strain value at 120 days for sample GPC500-8 was 652με. For AAGC, the autogenous shrinkage strain is approximately 50% to 60% of the drying shrinkage strain, whereas for OPCC, this value is around 18%.

As observed, the autogenous shrinkage strain of AAGC is up to seven to ten times greater than that of OPCC. In this experiment, the mixtures GPC400-6, GPC400-8, GPC400-10, GPC450-8, and GPC500-8 exhibit significant autogenous shrinkage strain of 502με (GPC400-6) to 652με (GPC500-8) at 120 days; while the mixtures O-405, O-461, and O-515 have the strain of 47με to 75με at 120 days. This could result from a higher degree of saturation, a finer pore structure, and greater chemical shrinkage in AAGC mixtures.

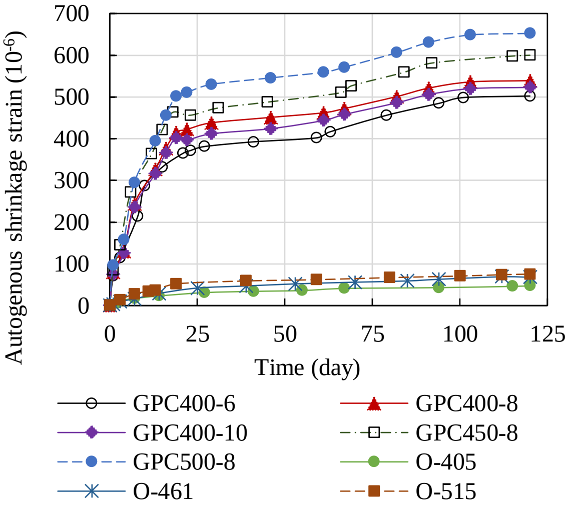

Fig. 9 Autogenous shrinkage strain

To investigate the effect of rebars on the drying shrinkage strain, test series TS-R- were conducted. A single bar with a diameter of 12 mm, corresponding to a reinforcement ratio of 1.13%, was placed in the centre of the specimens. Fig. 10 illustrates the comparison of drying shrinkage strain between the specimens with and without rebar for AAGC mixtures. At 120 days, the maximum drying shrinkage strain of GPC400-6 (without rebar) was 777με, while the strain of GPC400-6-TSR (with rebar) was only 174με, which is approximately 22% of the shrinkage strain of GPC400-6. The same trend was observed in other mixtures: the drying shrinkage strain of the mixtures with rebar was only about 20% to 23% of that without rebar. Thus, this experiment concludes that a reinforcement ratio of 1.13% can reduce the drying shrinkage strain of AAGC mixtures by approximately 4.0 to 5.0 times.

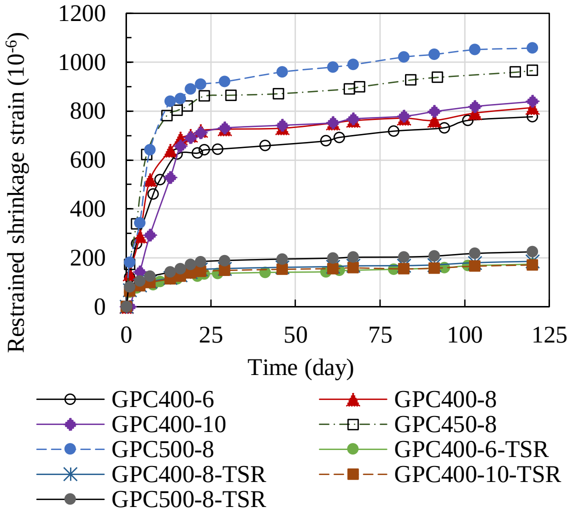

Fig. 10 Restrained shrinkage strain with rebar

4.2.1 Effect of alkali activator to FG ratio

The impact of the alkali activator (ACT) on the total amount of FA and GBFS (denoted as 'FG') is illustrated in Fig. 11. For the mixtures GPC400-6, GPC400-8, and GPC400-10, the ratio of water to FG remains constant at 0.45. The results indicate that an increase in the amount of ACT resulted in only a slight rise in drying shrinkage. When the ACT/FG ratio was modified from 6% to 8% and then to 10%, AAGC specimens exhibited 11% and 13% higher drying shrinkage at 60 days, and 5% and 9% higher drying shrinkage at 120 days. Therefore, the amount of alkali activator had a minimal effect on the drying shrinkage of AAGC.

4.2.2 Effect of total content of FG

The effect of the total amount of FA and GBFS (FG content) on drying shrinkage was examined by varying the FG content from 400 to 500 kg (GPC400-8, GPC450-8, and GPC500-8), while the ACT amount was fixed at 8%. The results in Fig. 11 illustrate that an increase in FG content led to significantly higher drying shrinkage. When the FG content changed from 400 to 450 and 500 kg, AAGC specimens experienced 18% and 30% greater drying shrinkage at 60 days, and 19% and 30% higher drying shrinkage at 120 days.

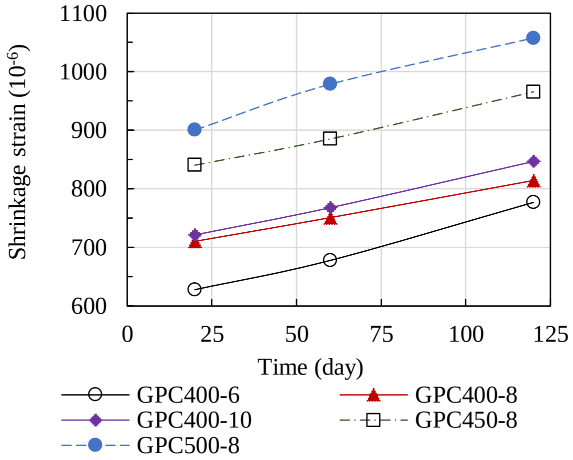

Fig. 11 Effect of ACT/FG ratio and total amount of FG on drying shrinkage

4.3 Comparison of Experimental Results With The Prediction Models

The American Concrete Institute (ACI) proposed a prediction model for shrinkage in ACI 209R-92 [23]. The primary inputs for predicting shrinkage are the age of loading, curing period, relative humidity, specimen size, slump, fine aggregate, cement content and type, and air content. This model is very straightforward to apply and is expressed by Eq. (3).

$$\varepsilon_{sh}\left(t,t_c\right)=\frac{t-t_c}{T_c+\left(t-t_c\right)}\varepsilon_{shu} \qquad (3)$$

For conditions other than the standard conditions, the average value of ultimate shrinkage must be adjusted using seven correction factors [23].

$$\varepsilon_{shu}=780\gamma_{sh}\times10^{-6} \qquad (4)$$

where $\gamma_{sh}=\gamma_{sh,tc}\gamma_{sh,RH}\gamma_{sh,vs}\gamma_{sh,s}\gamma_{sh,\psi}\gamma_{sh,c}\gamma_{sh,\alpha}$.

The prediction model according to EN 1992-1-1 [24] takes into account relative humidity, specimen form and size, and concrete compressive strength. It includes the autogenous shrinkage $\varepsilon_{ca}(t)$, the drying shrinkage $\varepsilon_{cd}(t)$, and can be presented by Eq. (5).

$$\begin{aligned}\varepsilon_{cs}(t)&=\varepsilon_{ca}(t)+\varepsilon_{cd}(t)\\ \varepsilon_{ca}(t)&=\beta_{as}(t)\times\varepsilon_{ca}(\infty)\\ \varepsilon_{cd}(t)&=\beta_{ds}(t,t_s)\times K_h\times\varepsilon_{cd,0}\end{aligned} \qquad (5)$$

The proposed model in Australian standard AS3600 [25] also incorporates compressive strength, environmental conditions and aggregate type. Total shrinkage strain ε_{cs} comprises autogenous shrinkage ε_{cse} and drying shrinkage ε_{csd} and it can be calculated by using Eq. (6).

$$\begin{aligned} \varepsilon_{cs} &= \varepsilon_{cse} + \varepsilon_{csd} \\ \varepsilon_{cse} &= \varepsilon^{*}_{cse}(1-e^{-0.1t}) \\ \varepsilon_{csd} &= K_1 K_4 \varepsilon_{cdsb} \end{aligned} \quad (6)$$

According to the CEB-Fib model 2010 [26], the total shrinkage $\varepsilon_{cs}(t,t_s)$ depends on concrete compressive strength, environmental humidity, age of loading, curing temperature and ratio of volume to surface of the specimen. It can be calculated by Eq. (7).

$$\varepsilon_{cs}(t,t_s) = \varepsilon_{cbs}(t) + \varepsilon_{cds}(t,t_s) \quad (7)$$

where $\varepsilon_{cbs}(t)$ is the basic shrinkage which occurs even if no moisture loss, and $\varepsilon_{cds}(t,t_s)$ is the additional drying shrinkage if moisture loss occurs.

$$\begin{aligned} \varepsilon_{cbs}(t) &= \varepsilon_{cbs0}(f_{cm})\beta_{bs}(t) \\ \varepsilon_{cds}(t,t_s) &= \varepsilon_{cds0}(f_{cm})\beta_{RH}(RH)\beta_{ds}(t-t_s) \end{aligned} \quad (8)$$

The experimental shrinkage results are compared with the prediction models and shown in Figs. 12-18.

As illustrated in Figs. 12-14, for the OPC design mixes, the AS3600 prediction model provides the closest results to the experimental data. However, a significant discrepancy remains. For O-405, the difference is approximately 10%, but this value increases with higher cement content (24% and 34% for OPC-461 and OPC-515, respectively). This may be due to the differing temperature and humidity conditions between the experiment and the model.

For GPC design mixes illustrated in Figs. 15-18, a significant discrepancy exists between the experimental results and the AS3600 prediction models, ranging from approximately 63% for GPC400-6 to 72% for GPC500-8.

The discrepancies between the experimental results and the code prediction may be due to differences in hydration products, materials, pore structure evolution, curing conditions, etc. Therefore, a new model to predict shrinkage strain for GPC under Vietnamese weather conditions is necessary.

4.4 Ring Test

The restrained shrinkage test (ring test) was performed for the design mixes GPC450-8, GPC500-8, O-461, and O-515.

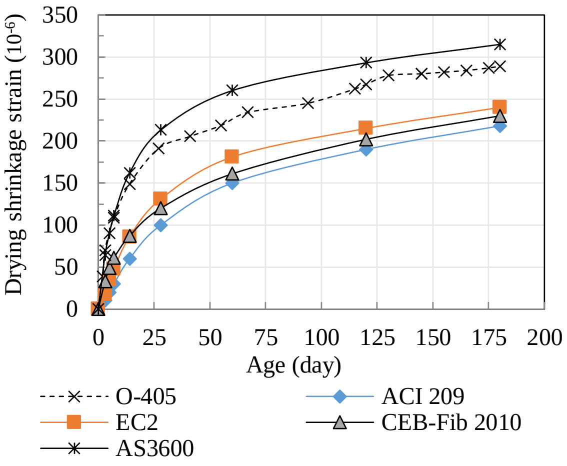

Fig. 12 Comparison of the drying shrinkage strain of OPC-405 with the prediction models

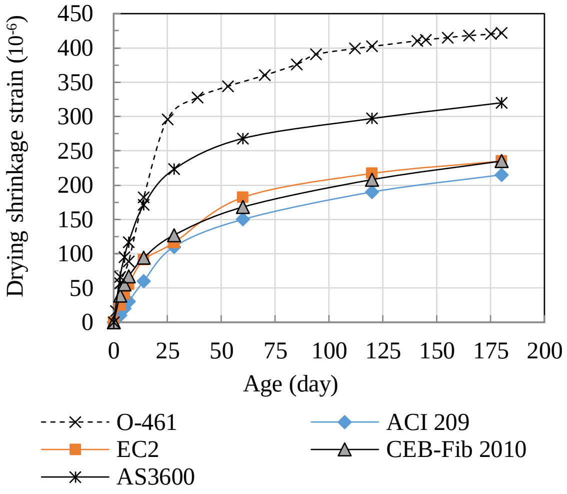

Fig. 13 Comparison of the drying shrinkage strain of OPC-461 with the prediction models

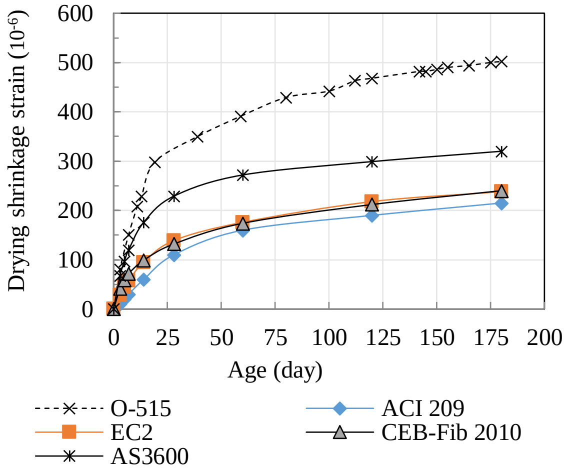

Fig. 14 Comparison of the drying shrinkage strain of OPC-515 with the prediction models

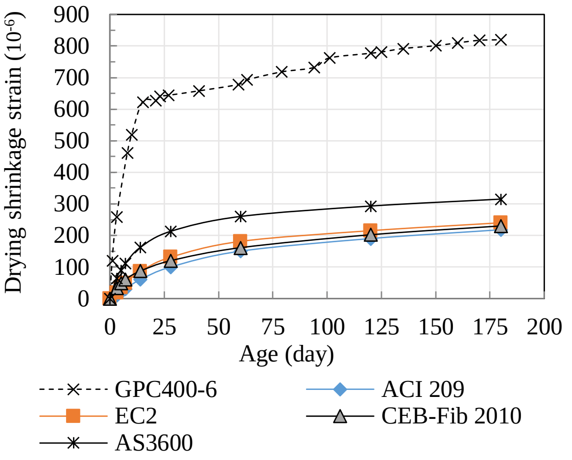

Fig. 15 Comparison of the drying shrinkage strain of GPC400-6 with the prediction models

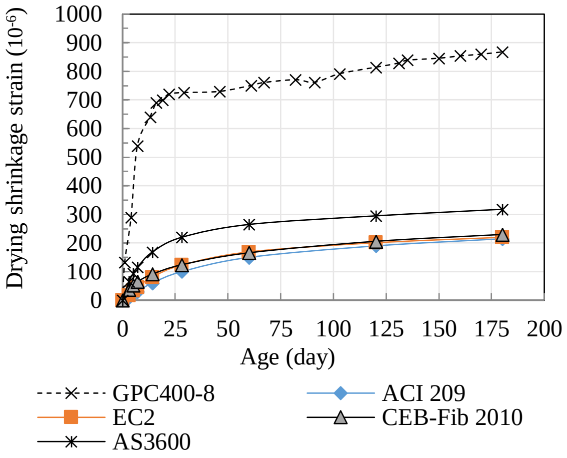

Fig. 16 Comparison of the drying shrinkage strain of GPC400-8

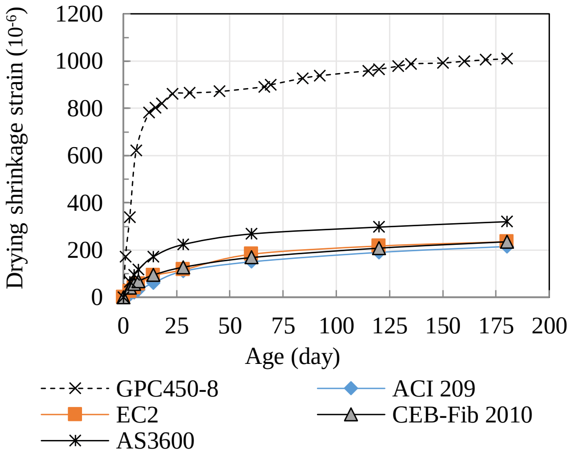

Fig. 17 Comparison of the drying shrinkage strain of GPC450-8

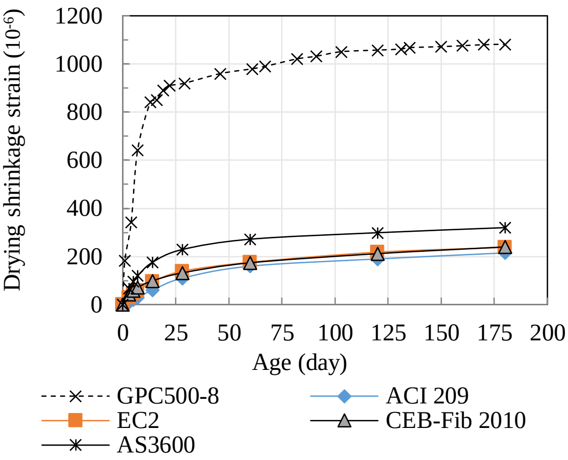

Fig. 18 Comparison of the drying shrinkage strain of GPC500-8

Fig. 19 presents the measured results of the ring tests from days 0 to 12. Previous studies [13, 27] showed that mix designs that remain intact longer without cracking are deemed to perform better than those that crack earlier. The ring samples begin to crack from the outer surface, with the crack gradually moving inward towards the ring over time. Once the crack reaches the ring, it results in the release of compressive stress on the steel ring. The speed at which the crack develops towards the ring is dependent on the mix design.

As shown in Fig. 19, for the OPC mixtures, the strain of the steel ring increased over time, reaching the highest strain of 49µm for O-515 and 40µm for O-461 at approximately 4.5 days. By 7 days, the crack width of the O-461 mix measured 0.16mm, while that of the O-515 mix was 0.17mm. The compressive stress in the ring dropped to zero when the crack fully propagated towards it.

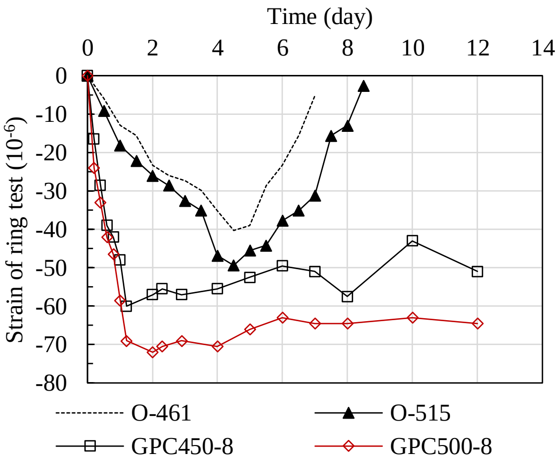

Fig. 19 Strain of steel ring against time

On the other hand, the maximum strain of the steel ring was 58.5µm at 1 day, and 72µm at 2 days for GPC450-8 and GPC500-8, respectively. The first crack in these GPC mixtures appeared earlier than in the OPC mixtures, with a crack width of 0.05 mm. However, after the first crack, other small cracks appeared and developed throughout the surface of the concrete ring; thus, compressive stress in the steel ring was still generated by the end of the test.

It can be concluded that OPC mixtures outperformed GPC in terms of the appearance of the first crack. The GPC mixtures developed cracks earlier, but they were small and did not propagate toward the steel ring.

5. CONCLUSIONS

This paper examines the drying, autogenous, and restrained shrinkage strains of five one-part alkali-activated geopolymer concrete mixtures. It investigates the concrete's compressive strength, the influence of mix design parameters, and two curing methods. Three OPC mixtures were cast for comparison purposes. The following conclusions can be drawn:

- The compressive strength of AAGC improved with rising calcium and silica content in the binder. The 28-day compressive strength of AAGC ranged from 31.6 MPa to 48.6 MPa.
- An increase in the alkaline activator from 6% to 10% can result in a 40.4% increase in compressive strength. Conversely, the amount of alkali activator had a minor impact on the drying shrinkage of AAGC.
- The 120-day drying shrinkage of AAGC specimens ranged from 815 με to 1058 με, approximately 2.3 to 4.0 times greater than OPCC samples.
- With an increase in the total amount of fly ash and ground blast furnace slag from 400 to 500 kg (25%), the drying shrinkage strain rose by approximately 30% at 120 days.
- An initial study in this paper indicated that employing a reinforcement ratio of 1.13% can reduce the drying shrinkage strain of AAGC by approximately 4.0 to 5.0 times. This merits further investigation.
- In this experiment, OPC mixtures outperformed GPC concerning the appearance of the first crack. While the GPC mixtures cracked earlier, the cracks were small and did not propagate towards the steel ring.

6. ACKNOWLEDGEMENT

The Development and Application of Advanced Materials and Modern Technologies in Construction (MTC) research group would like to express their gratitude to Hanoi University of Civil Engineering, Vietnam, for funding this research.

7. REFRENCES

[1] Davidovits J, Environmentally Driven Geopolymer Cement Applications, Conference proceedings, in Geopolymer 2002 Conference. Melbourne, Australia, 2002, p. 1-9.

[2] Pacheco-Torgal F., Abdollahnejad Z., Camões A.F., Jamshidi M., and Ding Y., Durability of alkali-activated binders: A clear advantage over Portland cement or an unproven issue?, Construction and Building Materials, Vol. 30, 2012, pp. 400-405. https://doi.org/10.1016/j.conbuildmat.2011.12.017

[3] Provis J.L., Alkali-activated materials, Cement and Concrete Research, 2018, 114: 40-48. https://doi.org/10.1016/j.cemconres.2017.02.009

[4] Luukkonen T., Abdollahnejad Z., Yliniemi J., Kinnunen P., and Illikainen M., One-part alkali-activated materials: A review, Cement and Concrete Research, Vol. 103, 2018, pp. 21-34. https://doi.org/10.1016/j.cemconres.2017.10.001

[5] Provis J.L., Geopolymers and other alkali activated materials: why, how, and what?, Materials and Structures, Vol. 47, Issue 1, 2014, pp. 11-25. https://doi.org/10.1617/s11527-013-0211-5

[6] Peng M.X., Wang Z.H., Shen S.H., and Xiao Q.G., Synthesis, characterization and mechanisms of one-part geopolymeric cement by calcining low-quality kaolin with alkali, Materials and Structures, Vol. 48, Issue 3, 2015, pp. 699-708. https://doi.org/10.1617/s11527-014-0350-3

[7] Zhou S., Tan C., Gao Y., Li Y., and Guo S., One-part alkali activated slag using Ca(OH)2 and Na_2CO_3 instead of NaOH as activator: more excellent compressive strength and microstructure, Materials Research Express, Vol. 8, Issue 8, 2021, pp. 55-67. https://dx.doi.org/10.1088/2053-1591/ac16f4

[8] Atiş C.D., Görür E.B., Karahan O., Bilim C., İlkentapar S., and Luga E., Very high strength (120MPa) class F fly ash geopolymer mortar activated at different NaOH amount, heat curing temperature and heat curing duration, Construction and Building Materials, Vol. 96, 2015, pp. 673-678. https://doi.org/10.1016/j.conbuildmat.2015.08.089

[9] Mao Y., Liu J., and Shi C., Autogenous shrinkage and drying shrinkage of recycled aggregate concrete: A review, Journal of

Cleaner Production, Vol. 295, 2021, 126435. https://doi.org/10.1016/j.jclepro.2021.126435

[10] Taghvayi H., Behfarnia K., and Khalili M., The Effect of Alkali Concentration and Sodium Silicate Modulus on the Properties of Alkali-Activated Slag Concrete, Journal of Advanced Concrete Technology, Vol. 16, Issue 7, 2018, pp. 293-305. https://doi.org/10.3151/jact.16.293

[11] Sadeghian G., Behfarnia K., and Teymouri M., Drying shrinkage of one-part alkali-activated slag concrete, Journal of Building Engineering, Vol. 51, 2022, 104263. https://doi.org/10.1016/j.jobe.2022.104263

[12] Zhang W., Hama Y., and Na S.H., Drying shrinkage and microstructure characteristics of mortar incorporating ground granulated blast furnace slag and shrinkage reducing admixture, Construction and Building Materials, Vol. 93, 2015, pp. 267-277. https://doi.org/10.1016/j.conbuildmat.2015.05.103

[13] Islam M.R., Ahmed M.K., Begum H.A., and Allouche E.N., Restrained Shrinkage of Fly Ash Based Geopolymer Concrete and Analysis of Long Term Shrinkage Prediction Models, Journal of the Arkansas Academy of Science, Vol. 71, Article 31, 2017. https://doi.org/10.54119/jaas.2017.7115

[14] BS EN 15167-1:2006 Ground granulated blast furnace slag for use in concrete, mortar and grout Definitions, specifications and conformity criteria. Brussels, Belgium. 2006.

[15] Thanh T.P., Nguyen T.T., and Nguyen T.T., Experimental Evaluation of Geopolymer Concrete Strength Using Sea Sand and Sea Water in Mixture, Civil Engineering Journal, Vol. 8, Issue 8, 2022, pp. 109-119. http://dx.doi.org/10.28991/CEJ-2022-08-08-03

[16] Trung N.-T., Minh P.-Q., Tung P.-T., and Phuong N.-V., Experimental study on mechanical and hydraulic properties of porous geopolymer concrete. International Journal of GEOMATE, Vol. 19, Issue 74, 2020, pp. 66-74. https://doi.org/10.21660/2020.74.41280

[17] Hadi M.N.S., Farhan N.A., and Sheikh M.N., Design of geopolymer concrete with GGBFS at ambient curing condition using Taguchi method. Construction and Building Materials, Vol. 140, 2017, pp. 424-431. https://doi.org/10.1016/j.conbuildmat.2017.02.131

[18] Bernal S.A., Mejía de Gutiérrez R., and Provis J.L., Engineering and durability properties of concretes based on alkali-activated granulated blast furnace slag/metakaolin blends, Construction and Building Materials, Vol. 33, 2012, pp. 99-108. https://doi.org/10.1016/j.conbuildmat.2012.01.017

[19] TCVN 3117:2022 Heavyweight concrete - Method for determination of shrinkage. TCVN. Hanoi. 2022.

[20] ASTM C1581/C1581M-24 Standard Test Method for Determining Age at Cracking and Induced Tensile Stress Characteristics of Mortar and Concrete under Restrained Shrinkage. 2024.

[21] Matalkah F., Salem T., Shaafaey M., and Soroushian P., Drying shrinkage of alkali activated binders cured at room temperature, Construction and Building Materials, Vol. 201, 2019, pp. 563-570. https://doi.org/10.1016/j.conbuildmat.2018.12.223

[22] Ma J. and Dehn F., Shrinkage and creep behavior of an alkali-activated slag concrete, Structural Concrete, Vol. 18, Issue 5, 2017, pp. 801-810. https://doi.org/10.1002/suco.201600147

[23] ACI 209.2R-08 Guide for Modelling and Calculating Shrinkage and Creep in Hardened Concrete. 2008.

[24] EN1992-1-1 Design of Concrete Structures – Part 1-1: General Rules and Rules for Buildings. 2004.

[25] AS 3600:2018 Concrete Structures. 2018.

[26] Convener W., FIB Model Code for Concrete Structures 2010, 1st ed. Special Activity Group 5 N.M.C.

[27] Bentz D.P., Quenard D.A., Baroghel-Bouny V., Garboczi E.J., and Jennings H.M., Modelling drying shrinkage of cement paste and mortar Part 1. Structural models from nanometres to millimetres, Materials and Structures, Vol. 28, Issue 8, 1995, pp. 450-458. https://doi.org/10.1007/BF02473164